

The metal-enriched host of an energetic γ -ray burst at $z \approx 1.6$ *

T. Krühler¹, J. P. U. Fynbo¹, S. Geier¹, J. Hjorth¹, D. Malesani¹, B. Milvang-Jensen¹, A. J. Levan², M. Sparre¹,
D. J. Watson¹, and T. Zafar¹

¹ Dark Cosmology Centre, Niels Bohr Institute, University of Copenhagen, Juliane Maries Vej 30, 2100 Copenhagen, Denmark
e-mail: tom@dark-cosmology.dk

² Department of Physics, University of Warwick, Coventry CV4 7AL, UK

Received 17 December 2011 / Accepted 1 August 2012

ABSTRACT

Context. The star-forming nature of long γ -ray burst (GRB) host galaxies provides invaluable constraints on the progenitors of GRBs and might open a short-cut to the characteristics of typical star-forming galaxies throughout the history of the Universe. Due to the absence of near-infrared (NIR) spectroscopy, however, detailed investigations, specifically a determination of the gas-phase metallicity of gamma-ray burst hosts, was largely limited to redshifts $z < 1$ to date.

Aims. We observed the galaxy hosting GRB 080605 at $z = 1.64$ using optical/NIR spectroscopy and high-resolution HST/WFC3 imaging in the rest-frame wavelength range between 1150 and 8700 Å. These data allow us to study a $z > 1$ GRB host in unprecedented detail and investigate the relation between GRB hosts and field galaxies.

Methods. We availed of VLT/X-shooter optical/NIR spectroscopy to measure the metallicity, electron density, star-formation rate (SFR), and reddening of the host of GRB 080605. Specifically, we used different strong-line diagnostics to robustly measure the gas-phase metallicity within the interstellar medium (ISM) for the first time based on [N II] at this redshift.

Results. The host of the energetic ($E_{\gamma, \text{iso}} \sim 2 \times 10^{53}$ erg) GRB 080605 at $z \sim 1.64$ is a morphologically complex, vigorously star-forming galaxy with an H α -derived SFR of $31^{+12}_{-6} M_{\odot} \text{ yr}^{-1}$. Its ISM is significantly enriched with metals. Specifically, [N II]/H α = 0.14 ± 0.02 , which yields an oxygen abundance $12 + \log(\text{O}/\text{H})$ between 8.3 and 8.6 depending on the adopted strong-line calibrator. This corresponds to values in the range of 0.4–0.8 Z_{\odot} . For its measured stellar mass ($M_{*} = 8.0^{+1.3}_{-1.6} \times 10^9 M_{\odot}$) and SFR, this value is consistent with the fundamental metallicity relation defined by star-forming field galaxies. The absence of strong Ly α emission constrains the escape fraction of resonantly-scattered Ly α photons to $f_{\text{esc}} \lesssim 0.08$.

Conclusions. Our observations provide a detailed picture of the conditions in the ISM of a highly star-forming galaxy with irregular morphology at $z \sim 1.6$. They include the first robust metallicity measurement based on [N II] for a GRB host at $z > 1$ and directly illustrate that GRB hosts are not necessarily metal-poor, both on absolute scales as well as relative to their stellar mass and SFR. GRB hosts could thus be fair tracers of the population of ordinary star-forming galaxies at high redshift.

Key words. gamma-ray burst: general – gamma-ray burst: individual: GRB 080605 – ISM: abundances – galaxies: star formation – galaxies: high-redshift

1. Introduction

The violent stellar explosion that gives rise to long γ -ray bursts (GRBs; see e.g., Piran 2004; Gehrels et al. 2009, for reviews) and their multi-wavelength afterglows has been firmly related to broad-line supernovae (SNe) of type Ic, and hence star-formation (SF), via the core-collapse of massive stars (e.g., Galama et al. 1998; Hjorth et al. 2003; Stanek et al. 2003; Malesani et al. 2004; Pian et al. 2006; Campana et al. 2006). The GRB's high-energy signature is very luminous, and unaffected by dust and therefore pin-points regions of star-formation irrespective of galaxy brightness, dust obscuration and redshift. GRB-selected galaxies hence provide a sample of high-redshift, star-forming galaxies that is fully complementary to conventional survey studies.

The luminous afterglows furthermore facilitate redshift measurements, and detailed investigation about the chemical composition (e.g., Savaglio et al. 2003; Prochaska et al. 2006, 2009; de Ugarte Postigo et al. 2010) and the dust properties of the host (e.g., Galama & Wijers 2001; Kann et al. 2006; Schady et al. 2007, 2010; Zafar et al. 2011). GRB hosts can hence be

targeted with a known redshift, position and information about the galaxy's interstellar medium (ISM) at hand, providing an independent diagnostic of galaxy evolution and star-formation.

Notably at the highest redshifts (Greiner et al. 2009; Tanvir et al. 2009; Salvaterra et al. 2009; Cucchiara et al. 2011), GRBs allow us to set observational constraints on the history of star-formation (e.g., Kistler et al. 2009; Robertson & Ellis 2012; Elliott et al. 2012), the galaxy luminosity function (Tanvir et al. 2012; Basa et al. 2012) as well as on the nature of young and star-forming galaxies (e.g., Christensen et al. 2004; Chen et al. 2009; Watson et al. 2011) beyond the detection limit of state-of-the-art surveys.

To represent a robust tool for cosmology and probe of star-formation, the physical conditions that lead to the formation of the GRB progenitor must be understood. As direct observations of GRB progenitors akin to those of some SNe remain impossible due to the cosmological distances, afterglow sight-line (e.g., Fynbo et al. 2009), spatially-resolved (e.g., Christensen et al. 2008; Thöne et al. 2008; Levesque et al. 2011) or galaxy-integrated measurements (e.g., Graham et al. 2009; Chen 2012) provide the most constraining information on the kind of galactic environments GRBs occur in.

However, the properties of an unbiased sample of long GRBs hosts are still largely unknown, and selection effects due

* Based on observations made with telescopes at the European Southern Observatory at La Silla/Paranal, Chile under program 087.B-0737(C).

to optically-dark bursts (Groot et al. 1998; Fynbo et al. 2001; Perley et al. 2009) arguably play a crucial role (e.g., Krühler et al. 2011; Perley et al. 2011a). Consequently, the conditions for the formation of GRBs, the relation between GRB hosts and field galaxies and the extent to which GRBs trace the cosmic star-formation rate (SFR) remain highly debated (e.g., Jakobsson et al. 2005; Fruchter et al. 2006; Kocevski et al. 2009; Campisi et al. 2011; Kocevski & West 2011).

Local galaxies hosting long GRBs tend to be of low stellar mass and metal content with respect to SDSS galaxies (Levesque et al. 2010a) as well as the hosts of core-collapse SNe (Fruchter et al. 2006; Modjaz et al. 2008), which has been interpreted as support for a limited chemical evolution of the GRB host – seemingly in line with metallicity constraints on the GRB progenitor from theoretical calculations based on the collapsar model (Woosley 1993; MacFadyen & Woosley 1999). These properties, however, are not indicative per-se of GRBs preferring low-metallicity environments, but instead could be the result of low-mass, low-metallicity galaxies dominating the local SFR (Mannucci et al. 2011). In fact, at higher redshifts (see e.g., Levan et al. 2006; Berger et al. 2007) and in *Swift* GRB host samples with a better controlled selection a population of red, luminous, high-mass hosts emerges (Rossi et al. 2012; Hunt et al. 2011; Chen et al. 2011; Svensson et al. 2012).

A fundamental characteristic of (GRB-selected) galaxies is their gas-phase metallicity, and in particular whether they follow the relation between stellar mass (M_*), metallicity (Z) and SFR defined by local field galaxies (Mannucci et al. 2010; Lara-López et al. 2010). However, observational access to the metallicity of GRB hosts remained largely elusive, and robust constraints are only available up to $z \sim 1$ (Savaglio et al. 2009; Levesque et al. 2010a). This is largely due to the absence of efficient near-infrared (NIR) spectrographs, as important tracers of metallicity (such as [N II] ($\lambda 6584$) and H α), are redshifted into the NIR wavelength regime above $z \sim 0.5$.

Here we present optical/NIR observations of the galaxy hosting GRB 080605 at $z = 1.64$ obtained with the X-shooter spectrograph at the Very Large Telescope (VLT), and NIR imaging with HST/WFC3 and LIRIS mounted at the *William Herschel* Telescope (WHT). The spectroscopic observations probe the rest-frame wavelength range between 1150 and 8700 Å and reveal a wealth of emission lines including H β , [O III], H α and [N II] ($\lambda 6584$).

GRB 080605 (Sbarufatti et al. 2008) was initially detected by the *Swift* satellite (Gehrels et al. 2004), and its optical/NIR afterglow was readily identified (Kann et al. 2008; Clemens et al. 2008). Spectroscopy of the afterglow was obtained with FORS2 at the VLT which yields a redshift of $z = 1.6403$ (Jakobsson et al. 2008; Fynbo et al. 2009). The optical/NIR afterglow is characterized by the presence of significant amounts of dust with $A_V \sim 0.5$ mag (Greiner et al. 2011; Zafar et al. 2011), including evidence of a 2175 Å feature (Zafar et al. 2012). The 2175 Å dust bump is a common characteristic observed along sight-lines through the Milky-Way. It becomes weaker in the Large Magellanic Cloud, and is absent from most sight-lines through the Small Magellanic Cloud. It is only rarely observed toward high-redshift environments such as quasars or absorbing systems, but common along sight-lines to highly extinguished afterglows (e.g. Krühler et al. 2008; Elíasdóttir et al. 2009; Zafar et al. 2011; Perley et al. 2011b). The carrier of the bump is currently not fully understood with graphite and polycyclic aromatic hydrocarbons being primary candidates (see e.g., Draine 2003, for a review).

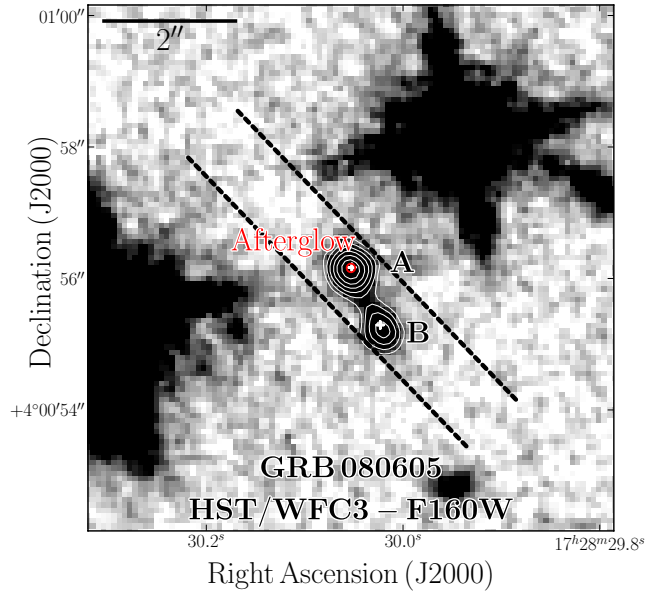


Fig. 1. Finding chart ($8'' \times 8''$) for the host of GRB 080605 as imaged with HST/WFC3. The afterglow position and its uncertainty are indicated by a red circle, and the different components are labeled A and B. The barycenter of each component is indicated by a white cross. The geometry of X-shooter’s UVB slit with width of $1''.0$ is illustrated by dashed black lines. The VIS and NIR slit have the same orientation but a width of $0''.9$. Logarithmically spaced contours are shown in white lines.

We adopt the concordance ($\Omega_M = 0.27$, $\Omega_\Lambda = 0.73$, $H_0 = 71 \text{ km s}^{-1} \text{ Mpc}^{-1}$) Λ CDM cosmology. All errors are given at 1σ confidence levels. All magnitudes are given in the AB system and are corrected for the Galactic reddening of $E_{B-V} = 0.137$ mag (Schlegel et al. 1998). The solar oxygen abundance is assumed to be $12 + \log(\text{O}/\text{H}) = 8.69$ (Asplund et al. 2009) throughout this work. Wavelengths are given in vacuum and the redshifts in the heliocentric system.

2. Observations and data reduction

2.1. Space-based imaging

The host of GRB 080605 was observed with the *Hubble* Space Telescope (HST) and Wide Field Camera 3 (WFC3) as part of a snapshot program targeting GRB hosts (PI: A. J. Levan, Proposal ID: 12307) on 2012-02-22. HST imaging (see Fig. 1) was obtained in the *F160W* filter in a three-point dither pattern resulting in a total exposure time of 1209 s. Individual images (pixel scale $0''.128/\text{px}$.) were drizzled to an output image with a pixel scale of $0''.08$ per pixel. Using several unsaturated stars in the field of view we measure a FWHM of the stellar PSF of 2.6 ± 0.1 px, which is $0''.21 \pm 0''.01$.

To accurately locate the position of the afterglow within its host, we first used a GROND afterglow image from Greiner et al. (2011) and calibrated it astrometrically against ~ 80 sources from the USNO catalog. This sets the absolute astrometric scale with an accuracy of around $0''.4$ in each coordinate. The uncertainty introduced by centroiding errors of the afterglow is ≈ 15 mas. Afterwards, we registered a deeper GROND host image (Krühler et al. 2011) against the afterglow image using common field stars. The mapping uncertainty between the two GROND images is 20 mas. Finally, we used fainter stars from the host image that are unsaturated in the WFC3 frame to tie the space- to the

Table 1. Photometric measurements.

Instrument	Filter	Exposure (s)	Brightness (mag) ^a
HST/WFC3	<i>F160W</i>	1209	(A) 22.38 ± 0.05
"	"	"	(B) 23.13 ± 0.06
"	"	"	(A and B) 21.96 ± 0.04
LIRIS	<i>J</i>	1980	(A and B) 22.2 ± 0.3
LIRIS	<i>K_s</i>	2520	(A and B) 21.8 ± 0.3

Notes. ^(a) All magnitudes are in the AB system and corrected for a Galactic foreground extinction corresponding to a reddening of $E_{B-V} = 0.137$ mag (Schlegel et al. 1998).

ground-based imaging. In the last step the RMS-scatter of stellar positions is 60 mas in each coordinate, which dominates the total relative accuracy (65 mas) of the position of the afterglow within its host.

The host of GRB 080605 is clearly extended in the N/E direction in the HST imaging, and consists of two, somewhat blended components A and B (Fig. 1) with a projected distance of 1''0 between the brightest pixel of each component (corresponding to 8.6 kpc at $z = 1.641$). Photometry (see Table 1) was derived using elliptical Kron magnitudes via SExtractor (Bertin & Arnouts 1996), an aperture correction of $6 \pm 4\%$ to the total flux (Graham & Driver 2005) and the tabulated HST/WFC3 zeropoints¹ from March 06, 2012. Deblending parameters were set one time to measure the integrated flux of the both components to be comparable to the ground based imaging, and a second time to measure the flux contribution of the individual host components (see also Table 1). Given the small angular separation, the two components are not resolved in our ground-based imaging.

2.2. Ground-based imaging

The field of the host of GRB 080605 was also imaged with the LIRIS instrument (Manchado et al. 2004) mounted at the 4.2 m WHT. We obtained a total of 0.55 h of exposures in the *J* (average FWHM of the stellar PSF is 1''4), and 0.70 h in the *K_s*-band (average FWHM of the stellar PSF is 1''0) at airmasses between 1.3 and 2.0. The data were reduced and photometry was performed within pyraf/IRAF (Tody 1993) in a standard manner. Absolute calibration was obtained against roughly 40 field stars with magnitudes from the 2MASS catalog. This procedure resulted in an absolute photometric accuracy of around 0.05 mag in the *J*, and 0.07 mag in the *K* band, which is negligible compared to the error introduced by photon statistics. The LIRIS photometry is summarized in Table 1.

2.3. X-shooter optical/NIR spectroscopy

X-shooter (D'Odorico et al. 2006; Vernet et al. 2011) at the VLT observed the host of GRB 080605 starting at 08:22 UT on 2011-04-26 for a total exposure time of 0.98 h in the ultraviolet/blue (UVB), 1.01 h in the visual (VIS), and 1.00 h in the NIR arm, respectively. Spectroscopy was obtained with slit widths of 1''0 (UVB), and 0''9 (VIS and NIR), which results in resolving powers of $\lambda/\Delta\lambda \approx 5100$, 8800 and 5100 for the three arms. The geometry of the slit is illustrated in Fig. 1.

Sky conditions were clear with an average seeing of 1''2. In total, four nodded exposures in the sequence ABBA were

obtained. In each nodding position a single UVB and VIS frame (885 and 910 s exposure time each), and three NIR frames (300 s exposure time each) were taken. Data were reduced with the X-shooter pipeline v. 1.5.0 (Goldoni et al. 2006) in physical mode, and the spectra were extracted using an optimal, variance-weighted method in IRAF (Tody 1993).

The wavelength-solution was obtained against ThAr arc-lamp frames leaving residuals of around 0.2 pixel which corresponds to 6 km s^{-1} at $10\,000 \text{ \AA}$. Flux-calibration was performed against the spectro-photometric standard LTT7987² observed during the same night at 09:46 UT, immediately after the science exposures.

The stellar continuum of the host of GRB 080605 is detected in the X-shooter spectrum with a $S/N \approx 0.3\text{--}0.9$ per pixel in parts of the UVB (3600 \AA to 5500 \AA) and VIS (5600 \AA to 9800 \AA). Within the NIR arm the continuum is only marginally seen in the *J* and *H* bands with $S/N \sim 0.1\text{--}0.2$ per pixel due to X-shooter's lower sensitivity in this wavelength range. The host is undetected in the wavelength range of the *K*-band with a S/N smaller than ~ 0.1 per pixel.

A robust flux-calibration within the broad wavelength range of X-shooter's sensitivity is challenging. We hence further corrected the flux-calibrated X-shooter spectrum in the UVB and VIS arms by integrating it over the filter curves of GROND (Greiner et al. 2008) and HST and matching it to the available host photometry (Krühler et al. 2011). This procedure results in scaling factors of around 1.63 ± 0.09 for the *g'*-band in the UVB arm ($\approx 4590 \text{ \AA}$), and 1.56 ± 0.13 , 1.35 ± 0.12 and 1.26 ± 0.14 for the *r'*, *i'* and *z'* band at 6220, 7640 and 8990 \AA , respectively. For the NIR arm, we derive factors of 1.4 ± 0.4 for the *J*-band and 1.4 ± 0.2 for the *F160W*-band. Due to the non-detection of the continuum in the *K*-band, no correction can be obtained between 18 000 and 23 000 \AA , but no emission lines are detected in this wavelength regime.

We further tested the absolute flux calibration and its inter- and intra-arm continuity via observations of telluric standard stars taken on the same night. We find that the absolute flux of the telluric is typically recovered within uncertainties of 30%, while its spectral shape is robust to an accuracy better than 15% within each arm.

3. Results

3.1. Host galaxy system and afterglow position

The system hosting GRB 080605 consists of two components A and B (see Fig. 1) with barycentric coordinates of $\text{RA}(J2000) = 17:28:30.05$, $\text{Dec}(J2000) = +04:00:56.2$ for component A and $\text{RA}(J2000) = 17:28:30.02$, $\text{Dec}(J2000) = +04:00:55.3$ for component B, respectively. The half-light radii r_e in the observed *F160W*-band (rest-frame $\sim 5800 \text{ \AA}$) for the two components are marginally resolved ($r_{e,5800 \text{ \AA}}^A \sim 0''.19$ or 1.6 kpc, $r_{e,5800 \text{ \AA}}^B \sim 0''.26$ or 2.2 kpc). The half-light radius for the total host complex is $r_{e,5800 \text{ \AA}} = 0''.41$ or 3.5 kpc.

The afterglow position coincides with the center of component A (Fig. 1). Within our astrometric accuracy of 65 mas, no significant offset is detected and we conclude that the GRB exploded within a projected distance of 900 pc (90% confidence) to the central region of component A.

¹ http://www.stsci.edu/hst/wfc3/phot_zp_lbn

² http://www.eso.org/sci/facilities/paranal/instruments/xshooter/tools/specphot_list.html

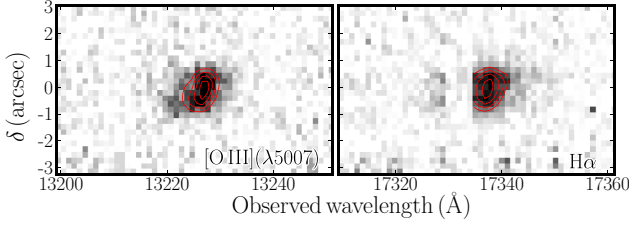


Fig. 2. Two-dimensional cutouts of the X-shooter NIR spectrum centered on the observed wavelength of [O III](λ 5007) and H α . Skylines are indicated with gray shading. Linearly spaced contours are shown in red lines.

Table 2. Host parameters from stellar population synthesis modeling.

Absolute magnitude M_B (mag _{AB})	-22.4 ± 0.1
Age (Gyr)	$0.19^{+0.09}_{-0.10}$
Effective reddening E_{B-V}^{stars} (mag)	$0.10^{+0.05}_{-0.08}$
M_* ($10^9 M_\odot$)	$8.0^{+1.3}_{-1.6}$
SFR _{SED} ($M_\odot \text{ yr}^{-1}$)	49^{+26}_{-13}
sSFR _{SED} (Gyr^{-1})	6^{+5}_{-2}

3.2. Emission line profile

The X-shooter spectrum of the host galaxy of GRB 080605 covers the wavelength range between 3050 and 23 000 Å (rest-frame 1150 and 8700 Å) and is rich in emission lines. The emission lines are identified as the doublets of [O II], [O III], [S II], [N II], as well as H α , H β , and [O I]. The significance of the detection of the Balmer lines, [O III], [O II] and [N II] (λ 6584) is $>8\sigma$, while it is between 2 and 4σ for [N II] (λ 6548), the [S II] doublet, and [O I] (λ 6366).

The two emission lines detected at the highest S/N ([O III] (λ 5007) and H α , see also Sect. 3.4) are marginally tilted, reflecting the contributions of component A and B. Figure 2 shows the two-dimensional cutouts centered at the wavelength of the [O III] (λ 5007) and H α lines. They define heliocentric³ redshifts of $z_A = 1.64104 \pm 0.00004$ and $z_B = 1.64083 \pm 0.00007$ measured from the peak of the emission lines. These values correspond to a separation of $\Delta v \sim 20 \text{ km s}^{-1}$ (Figs. 1 and 2).

For the fainter emission lines, we lack signal-to-noise ratio (S/N) in our X-shooter spectrum and individual contributions of components A and B are strongly blended and can not be resolved. Similar to the ground-based photometry, we will thus report line-fluxes integrated over the complete host galaxy complex (Sect. 3.4) in the following.

3.3. Host SED

Fitting the HST and LIRIS NIR photometry of the entire host system together with published broad-band magnitudes (see Krühler et al. 2011, for details) in LePhare⁴ (Arnouts et al. 1999; Ilbert et al. 2006) yields the galaxy parameters listed in Table 2. Here we assumed models from Bruzual & Charlot (2003) based on an initial mass function (IMF) from Chabrier (2003) and a Calzetti dust attenuation law (Calzetti 2001). Given that both method and data are largely unchanged, these values are only

³ The heliocentric correction in the direction of GRB 080605 is 19 km s^{-1} for our observations.

⁴ <http://www.cfht.hawaii.edu/~arnouts/lephare.html>

Table 3. Emission lines in the X-shooter spectrum.

Transition	Wavelength ^a	Flux ^b	Correction ^c
Ly α	1215	<4.7	$3.2^{+7.8}_{-1.6}$
[O II]	3727	10.6 ± 0.6	$1.7^{+1.3}_{-0.5}$
[O II]	3730	12.2 ± 0.9	$1.7^{+1.3}_{-0.5}$
H β	4863	7.2 ± 0.5	$1.8^{+1.1}_{-0.6}$
[O III]	4960	6.5 ± 0.4	$1.8^{+1.0}_{-0.6}$
[O III]	5008	21.6 ± 0.6	$1.8^{+1.0}_{-0.6}$
[O I]	6366	1.6 ± 0.4	$1.7^{+0.7}_{-0.4}$
[N II]	6550	0.8 ± 0.4	$1.6^{+0.6}_{-0.3}$
H α	6565	22.4 ± 1.0	$1.6^{+0.6}_{-0.3}$
[N II]	6585	3.2 ± 0.4	$1.6^{+0.6}_{-0.3}$
[S II]	6718	1.2 ± 0.4	$1.6^{+0.6}_{-0.3}$
[S II]	6733	0.9 ± 0.4	$1.6^{+0.6}_{-0.3}$

Notes. ^(a) Rest-frame vacuum wavelength in units of Å. ^(b) Galactic extinction corrected flux in units of $10^{-17} \text{ erg s}^{-1} \text{ cm}^{-2}$. The flux is quoted as measured in the X-shooter spectrum (without correction). The flux error is statistical only, and does not contain the error of the absolute flux calibration. ^(c) The given correction includes the matching factor to broad-band photometry, stellar Balmer absorption if applicable, and reddening according to the Balmer line ratio. These factors are not independent. In particular it was assumed that [N II] and H α , for example, have identical values (except for the Balmer absorption).

slightly refined with respect to those computed by Krühler et al. (2011).

3.4. Emission line fluxes

In the measurement of emission line fluxes (Table 3), the redshift (i.e., line centroids) and line widths were fitted simultaneously by tying weak emission lines to those detected at high S/N. In detail, we linked the parameters of the two components of the [O II] doublet in the visual arm, as well as the Gaussian widths and centroids of the various emission lines in the NIR arm. Although the emission of the forbidden and recombination lines does not necessarily arise from the same physical components, the assumption of a common redshift and line width provides a fair approximation and a good fit to the data (Fig. 3). The robustness of the procedure is further supported by, within errors, unchanged line parameters, fluxes and flux ratios when using different combination of ties (i.e., free FWHM, tying H β to [O III] (λ 5007) or all lines except [O II] to each other) or allowing for multiple Gaussian components in the individual lines.

In addition, we cross-checked our method by numerically integrating the flux of the emission lines. Here, errors were estimated via Monte-Carlo techniques. This results in values that are consistent with those of the Gaussian fitting at 2σ confidence, but is more sensitive to skylines and small-scale irregularities in the data. It further disregards the physical information of a common redshift, and hence results in larger errors than the Gaussian fitting in particular for lines with low S/N, or those affected by skylines. We thus report fit-based values in Table 3. Our conclusions remain unchanged when using different Gaussian fitting methods or numerical integration techniques for the line flux measurements.

From the observed FWHM of the [O II] doublet ($\approx 5 \text{ \AA}$), and assuming a resolving power of 8800 of X-shooter's VIS arm,

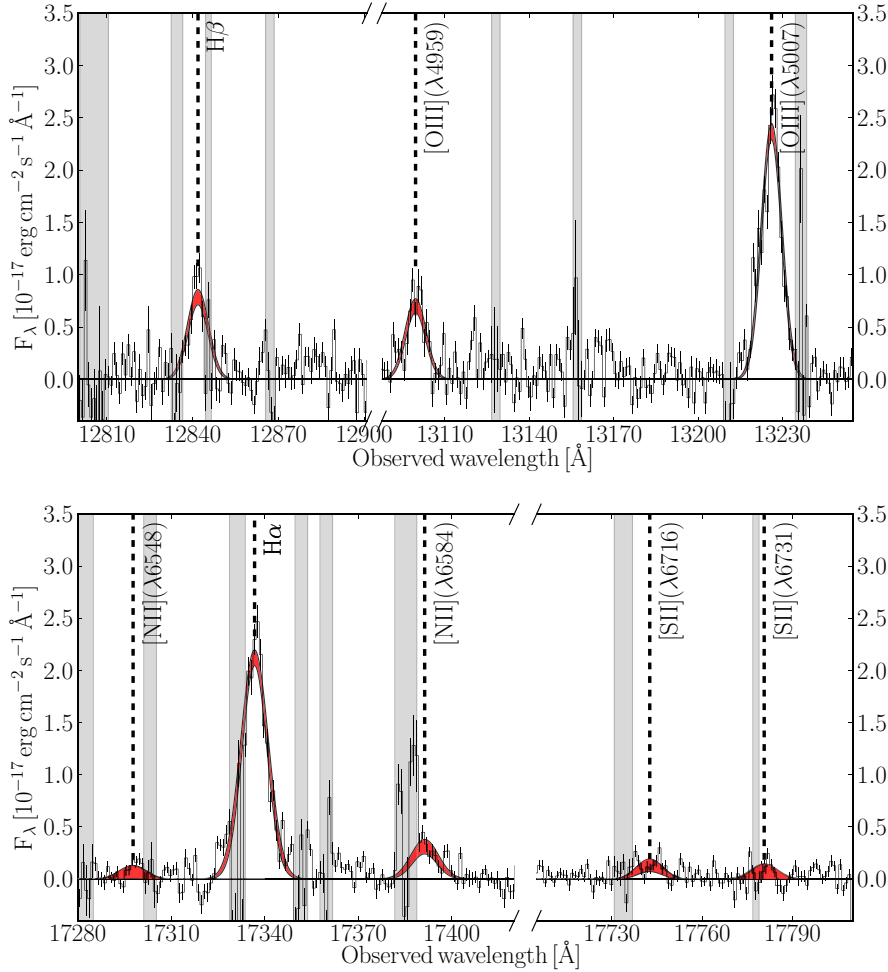


Fig. 3. Continuum-subtracted emission lines used to determine the gas-phase metallicity in the X-shooter spectrum, as well as the [S II] doublet. The black line shows the raw spectrum including errors, and the red-shaded areas denote the 90% confidence region of the fit of the emission lines using Gaussians. Grey shaded areas denote wavelength regions that have been omitted in the fitting due to skyline contamination.

we derive a measured velocity dispersion σ of around $\sigma \sim 50 \text{ km s}^{-1}$ for the host galaxy complex, comparable to star-forming systems of similar mass observed through gravitational lenses (e.g., Christensen et al. 2010).

We do not detect significant emission from the resonant Ly α transition. Using the redshift, and assuming an intrinsic FWHM of twice the recombination lines (e.g., Fynbo et al. 2010), we set a limit on the Ly α flux of $4.7 \times 10^{-17} \text{ erg cm}^{-2} \text{ s}^{-1}$ ($7.6 \times 10^{-17} \text{ erg cm}^{-2} \text{ s}^{-1}$ after matching the spectrum to photometry) at the redshifted Ly α wavelength of 3210 \AA . It is estimated from an artificial emission line added on top of the sky contribution at the respective wavelength range, folded with the error spectrum and represents the flux that is detected at a combined $S/N > 3$ in 99% of all iterations. Similar limits are obtained when allowing for an offset of several ten to few hundreds of km s^{-1} for Ly α with respect to the recombination lines (Milvang-Jensen et al. 2012). The non-detection of Ly α is further discussed in Sect. 4.4.

In the further analysis, we matched the spectrum to broadband photometry (see Sect. 2.3), and applied when appropriate the correction for an average stellar Balmer absorption using a rest-frame equivalent width of 1 \AA (Cowie & Barger 2008; Zahid et al. 2011), and for host galaxy extinction using the Balmer decrement (see Sect. 3.5). The corresponding wavelength-dependent factors are shown in Table 3.

Comparing the emission line ratios of [O III]/H β versus [N II] ($\lambda 6584$)/H α against standard diagnostic relations (e.g., Kewley et al. 2001; Kauffmann et al. 2003), a significant contribution of an AGN to the host emission of GRB 080605 is readily excluded. Measurements of emission line fluxes and upper limits are reported in Table 3.

3.5. Balmer decrement

The ratio between the Balmer lines H α and H β is a tracer of the visual extinction toward the H II regions. We used the respective photometry-matched and stellar Balmer absorption corrected line fluxes to derive the intrinsic Balmer ratio, which is a direct measure of the selective reddening, or the total visual extinction under the assumption of a specific extinction law (and treating the H II regions as point-like). This probes a different physical quantity than the reddening value inferred from fitting the galaxy’s spectral energy distribution (SED) from Table 2, as the SED modeling is sensitive to the attenuation of the stellar component which depends on the topology of the ISM and dust and galaxy geometry (e.g., Pierini et al. 2004).

Under standard assumptions of electron density ($10^2 \text{ cm}^{-3} \lesssim n_e \lesssim 10^4 \text{ cm}^{-3}$, see also Sect. 3.6) and temperature ($T_e \sim 10^4 \text{ K}$) for case B recombination (Osterbrock 1989), the Balmer ratio indicates an average reddening toward the H II regions of

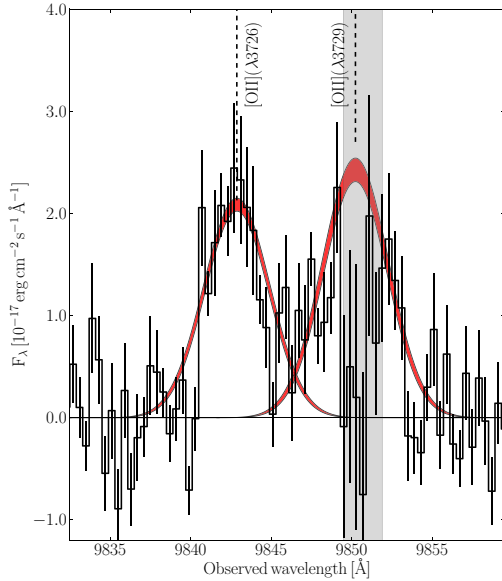


Fig. 4. The continuum-subtracted [O II] ($\lambda\lambda 3726\ 3729$) doublet. Lines and shadings are the same as in Fig. 3.

$E_{B-V}^{\text{gas}} = 0.07^{+0.13}_{-0.07}$ mag. This corresponds to $A_V^{\text{gas}} = 0.22^{+0.40}_{-0.22}$ mag when assuming a MW-type extinction law with $R_V = 3.1$ (Cardelli et al. 1989). The reddening corrections according to the Balmer decrement for all emission lines except Ly α are fairly robust and independent on the assumption of a specific extinction law, as there is little difference within the wavelength range of the Balmer lines between sight-lines through local galaxies (e.g., Pei 1992) or with respect to extra-galactic extinction laws derived from GRB afterglows (Schady et al. 2012).

3.6. Electron density

The flux ratio between the two components of the [O II] doublet is sensitive to the electron density (Osterbrock & Ferland 2006). Individual components are resolved and well detected because of the high spectral resolution of X-shooter (see Fig. 4). Assuming an electron temperature T_e of 10^4 K, we derive an electron density of $n_e \sim 200 \text{ cm}^{-3}$. This value is typical for Galactic H II regions (e.g., Copetti et al. 2000). The low significance of the detection of the [S II] doublet (see Fig. 3) prevents meaningful constraints on the electron density based on [S II].

3.7. Star-formation rate

Emission line fluxes of H α and [O II], as well as the UV continuum flux trace the un-obscured star-formation within a galaxy (Kennicutt 1998; Kewley et al. 2004). The H α -derived value presents the most reliable optical indicator of a galaxy's SFR, as it is independent of metal abundances, and less sensitive to the uncertainties in the visual extinction than the other methods. SFR values depend quite strongly on the assumption of the IMF. In the following, we report values based on the initial formulation of the SFR from Kennicutt (1998), but converted to a Chabrier IMF (Chabrier 2003)⁵. Based on H α , the SFR of the host of GRB 080605 is $\text{SFR}_{\text{H}\alpha} = 31^{+12}_{-6} M_{\odot} \text{ yr}^{-1}$. Here we used correction-factor and its error (see Tab. 3), and thus include the uncertainty in the flux calibration and host-intrinsic reddening.

⁵ Assuming a Salpeter IMF would increase all SFR estimates by a factor of ≈ 1.7 (e.g., Förster Schreiber et al. 2009).

SFRs from [O II] ($\text{SFR}_{[\text{O II}]} = 55^{+55}_{-22} M_{\odot} \text{ yr}^{-1}$) and the SED modeling ($\text{SFR}_{\text{SED}} = 49^{+26}_{-13} M_{\odot} \text{ yr}^{-1}$) are within the larger uncertainties in good agreement with the H α -derived value.

Optically derived SFRs do not provide a full picture of the total (obscured and unobscured) star-formation in a galaxy. Based on sub-mm and radio measurements, there is evidence that the total SFR of few GRB-selected galaxies can be around or even higher than $100 M_{\odot} \text{ yr}^{-1}$ (e.g., Berger et al. 2003; Tanvir et al. 2004; Michałowski et al. 2012). The sample of sub-mm detected GRB hosts, however, is still very limited (e.g., Michałowski et al. 2008), and a full census of the actual SFR of GRB hosts will have to await the advent of statistically representative samples observed with sensitive far-infrared, sub-mm or radio observatories such as *Herschel*, ALMA or the eVLA.

Despite these limitations, optically-derived SFRs are well-established tools for the characterization of galaxies. We will thus put the host of GRB 080605 into the context of SFRs from field galaxies derived in a similar manner, with the caveat that the reported SFRs might trace only a fraction of the total SFR of a given galaxy.

Together with the stellar mass measurement of $M_* = 8.0^{+1.3}_{-1.6} \times 10^9 M_{\odot}$, the specific SFR ($\text{sSFR}_{\text{H}\alpha} = \text{SFR}_{\text{H}\alpha}/M_*$) and growth timescale $\tau = 1/\text{sSFR}_{\text{H}\alpha}$ are 4 Gyr^{-1} and 260 Myr, respectively, making the host of GRB 080605 a highly active and star-bursting galaxy.

3.8. Metallicity

The gas-phase metallicity of galaxies is typically measured using different diagnostic ratios of emission lines originating in H II regions (see e.g., Kewley & Ellison 2008, and references therein). Most commonly used are the R_{23} calibrator, that requires measurements of line fluxes from [O II], [O III] and H β (Pagel et al. 1979; McGaugh 1991; Kobulnicky & Kewley 2004), the O3N2 and N2 diagnostics which uses ratios of [O III], and H β , and/or [N II] and H α (Alloin et al. 1979; Pettini & Pagel 2004), and the N2O2 indicator via [O II] and [N II] (Kewley & Dopita 2002). For a detailed description on the individual strong-line diagnostics we refer to Kewley & Ellison (2008).

The R_{23} method is double-valued but its degeneracy can be broken via the line ratios of [N II]/H α or [N II]/[O II]. In our case, [N II]/H $\alpha = 0.14 \pm 0.02$ and [N II]/[O II] = 0.10 ± 0.04 . The significant flux detected in [N II] strongly points to the upper branch solution. Similarly, the N2O2 ratio is only applicable for high metallicities with $\log([\text{N II}]/[\text{O II}]) > -1.2$. Due to the large difference in wavelength of the lines used by N2O2 and R_{23} , their values are sensitive to the reddening in the host and wavelength-dependent errors in the flux calibration.

Both the O3N2 (see Eq. (1)) and N2 methods, however, use flux ratios of adjacent emission lines, which are relatively close in wavelength space, and in our case are all within the NIR arm. The observed lines of [O III] and H β are located in the J , and [N II] and H α in the H -band. Errors in the flux calibration or systematic uncertainties due to flat-fielding, slit-losses, intrinsic host extinction or reddening in the Galaxy are hence not going to affect the overall metallicity measurement in this case.

Based on O3N2, for example, the oxygen abundance is (Pettini & Pagel 2004):

$$12 + \log(\text{O}/\text{H}) = 8.73 - 0.32 \times \log\left(\frac{F_{[\text{O III}](\lambda 5007)}/F_{\text{H}\beta}}{F_{[\text{N II}](\lambda 6584)}/F_{\text{H}\alpha}}\right) \quad (1)$$

which is $12 + \log(\text{O}/\text{H}) = 8.31 \pm 0.02$ for GRB 080605. Using the N2, R_{23} and N2O2 strong-line indicators, the oxygen

Table 4. Oxygen abundances based on different strong-line indicators.

Indicator	Lines/methods	$12 + \log(\text{O}/\text{H})$	Z/Z_{\odot}	Uncertainty ^a (dex)	References
R_{23}	[O II](3727), H β , [O III](5007)	$8.45^{+0.09}_{-0.12}$	0.63 ± 0.15	0.15	(1), (2), (3)
	[O II](3727), H β , [O III](5007)	$8.50^{+0.10}_{-0.13}$	0.64 ± 0.17	~ 0.1	(4, 6)
O3N2	H β , [O III](5007), H α , [N II](6584)	8.31 ± 0.02	0.42 ± 0.02	0.14	(5)
	[O III](5007), [N II](6584)	8.46 ± 0.10	$0.59^{+0.15}_{-0.12}$	0.24	(6)
N2	H α , [N II](6584)	8.36 ± 0.03	0.47 ± 0.04	0.18	(5)
	H α , [N II](6584)	8.52 ± 0.06	$0.68^{+0.09}_{-0.08}$	0.12	(6)
N2O2	[O II](3727), [N II](6584)	$8.60^{+0.11}_{-0.19}$	$0.82^{+0.24}_{-0.29}$	~ 0.1	(7)
	[O II](3727) [N II](6584)	$8.53^{+0.14}_{-0.24}$	$0.69^{+0.27}_{-0.30}$	0.10	(6)
Combined fit	R_{23} , O3N2, N2, N2O2	8.52 ± 0.09	$0.68^{+0.15}_{-0.13}$	included	(4), (6), (8)

Notes. ^(a) Systematic 1σ scatter inherent to the diagnostic line ratio.

References. For the indicator: (1) Pagel et al. (1979); (2) McGaugh (1991); (3) Kobulnicky & Kewley (2004); (4) Maiolino et al. (2008); (5) Pettini & Pagel (2004); (6) Nagao et al. (2006); (7) Kewley & Dopita (2002); (8) Mannucci et al. (2011).

abundance is $12 + \log(\text{O}/\text{H}) = 8.36 \pm 0.03$ for N2, $12 + \log(\text{O}/\text{H}) = 8.45^{+0.09}_{-0.12}$ for R_{23} , and $12 + \log(\text{O}/\text{H}) = 8.60^{+0.11}_{-0.19}$ for N2O2. Here, all errors are based on the uncertainties of the line flux measurement and the correction factor only (see Table 3), and do not include the systematic error inherent to the calibrator. Errors correctly reflect the larger uncertainty in the strong-line diagnostics that include flux ratios between lines in different wavelength regimes (R_{23} and N2O2). Oxygen abundances based on different indicators are further summarized in Table 4. We use the appropriate diagnostics when comparing to literature values.

4. Discussion

The metallicity of GRB hosts is measured either directly in absorption using the bright afterglow emission, or, as in this work, in emission via host galaxy spectroscopy and strong-line diagnostics. In the former case, measurements are typically restricted to $z \gtrsim 2$ (e.g., Jakobsson et al. 2006; Savaglio 2006), while the latter case requires NIR spectroscopy for $z \gtrsim 1$. Emission line metallicities are calibrated on local samples, and hence depend on the assumption that the physical processes underlying these diagnostic ratios are still valid at high redshift. There is hence considerable systematic uncertainty between metallicities derived directly in absorption or through emission lines. Furthermore, metallicity measurements at high-redshift via the different techniques are available for only a few objects. They tend to agree reasonably well (see e.g., Dessauges-Zavadsky et al. 2010), but systematic effects in a direct comparison remain hard to quantify until larger samples of objects with both, ISM as well as gas-phase metallicities, become available.

Our measurement of the gas-phase metallicity of the host of GRB 080605 represents a first view into the metal abundances of GRB hosts in the redshift range $1 \lesssim z \lesssim 2$ (Fig. 5). Generally, the distribution in metallicity as inferred from GRB-DLAs shows a large dispersion with values $0.01 \lesssim Z/Z_{\odot}$ (Vreeswijk et al. 2004; Prochaska et al. 2008; Rau et al. 2010) to solar or even super-solar (Prochaska et al. 2009; Savaglio et al. 2003, 2012). A similar spread in metallicities is also found in hydrodynamical solutions of individual sight-lines through GRB hosts (Pontzen et al. 2010). The metallicity derived from afterglow spectroscopy could be dominated by sight-line effects, and large samples might be required to assess the general

properties of GRB hosts via afterglow spectroscopy in a statistical approach.

Host-integrated metallicities via emission lines should therefore give a more self-contained picture of the metal-enrichment of the ISM in high-redshift GRB hosts. Galaxy metallicity measurements are however challenging observationally in a stellar mass range around or below $10^{10} M_{\odot}$, and thus still sparse, in particular at $z > 1$. Current GRB host samples are furthermore subject to complex selection biases (Krühler et al. 2011), which are only resolved through statistical samples of high completeness (e.g., Fynbo et al. 2009; Cenko et al. 2009; Greiner et al. 2011; Salvaterra et al. 2012; Hjorth et al. 2012). Consequently, a consistent picture of the relation between galaxies selected through GRBs and normal field galaxies is not yet reached.

4.1. The host of GRB 080605 within the sample of GRB hosts

With respect to previous GRB host galaxies, the metallicity, stellar mass and SFR of the host of GRB 080605 are relatively high (see Fig. 5). With a metallicity around half solar, a stellar mass of $8 \times 10^9 M_{\odot}$ and SFR $\sim 30 M_{\odot} \text{ yr}^{-1}$, it is significantly enriched with metals and vigorously forming stars. This contradicts the suggestion, that an upper metallicity limit⁶ for cosmological, $z \gtrsim 1$, GRBs of $Z \lesssim 0.2 Z_{\odot}$ exists (Stanek et al. 2006).

The substantial gas-phase metallicity of the host is even more intriguing, as GRB 080605 itself is energetic. The inferred isotropic-equivalent energy release in γ -rays is $E_{\gamma, \text{iso}} \sim 2.2 \times 10^{53}$ erg as calculated from the prompt emission data from Golenetskii et al. (2008). This value puts GRB 080605 within the most-energetic 15% of all *Swift* bursts (Butler et al. 2007, 2010).

A connection between host metallicity and γ -ray energy release of the GRB, or a metallicity cut-off might be expected in the collapsar scenario (Woosley 1993; MacFadyen & Woosley 1999), for example. Progenitor stars with lower metallicities are likely to have higher angular momentum due to smaller wind losses, and thus result in a more energetic explosion (e.g., Hirschi et al. 2005; Yoon & Langer 2005). An energetic burst such as GRB 080605 would hence be more likely in a low-metallicity environment, in contrast to our observations.

⁶ Adopted to our reference solar oxygen abundance.

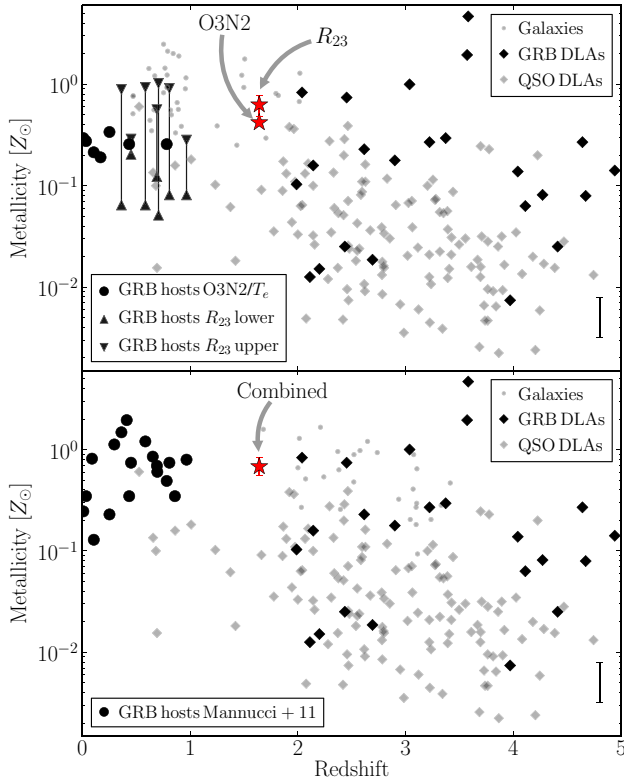


Fig. 5. Metallicity of the host of GRB 080605 (star). Other GRB host metallicities are shown with black circles and upward/downward triangles as compiled and in the scale of Savaglio et al. (2009) (top panel) and Mannucci et al. (2011) (bottom panel). Field galaxies are shown as gray dots (Savaglio et al. 2005; Pérez-Montero et al. 2009; Mannucci et al. 2009; Hayashi et al. 2009; Richard et al. 2011), and in similar metallicity scales as the GRB measurements. Absorption metallicities from GRB afterglows (Rau et al. 2010; D’Elia et al. 2010; Savaglio et al. 2012; Thöne et al. 2012, and references therein) and QSOs (Prochaska et al. 2003) are plotted as black and gray diamonds, respectively. Errorbars for individual events in the comparison samples are omitted to enhance clarity. The error bars at the bottom right corner of each panel illustrate uncertainties of 0.2 dex, which are typical for both, GRB-DLA (e.g., Rau et al. 2010; Thöne et al. 2012) and GRB host metallicity (e.g., Mannucci et al. 2011) measurements.

Our observations are, however, in line with the work of Wolf & Podsiadlowski (2007) and Levesque et al. (2010b), who find no correlation between $E_{\gamma, \text{iso}}$ and host metallicity in 18 GRBs at $z < 1$.

The role of metallicity in long GRB progenitors is thus far from being understood. The metallicity distribution of a representative GRB host sample will indirectly also allow us to put constraints on the metal content of the progenitor. For example, complex scenarios of stellar evolution, or binary models for the formation of long GRBs (e.g., Fryer et al. 1999) can both relax the constraints on progenitor metallicity. In addition, even within a metal-rich galaxy a metal-poor progenitor could in principle form in specific regions of fairly primordial chemical composition such as gas inflows or in (merging) galaxies with substantial diversity in their metal enrichment. To first order, however, the gas-phase, i.e., H II-region averaged, metallicity should provide a fair representation of the chemical evolution of the galaxy as a whole.

The galaxy hosting GRB 080605 has indeed a disturbed morphology, indicative of an early merger or intrinsically clumpy structure. A merger could have also triggered the enhanced

star formation of the host of GRB 080605 when compared to GRB hosts at low redshift (e.g., Savaglio et al. 2009; Levesque et al. 2010a). GRB hosts with similar SFR, however, might not be uncommon at $z > 1$. A good fraction of X-ray selected GRB hosts at $1 < z < 2$ has observed R -band brightnesses (probing the rest frame UV) in a range between 24 mag and 22.5 mag (Malesani et al. 2009) indicating dust un-corrected SFRs up to $10 M_{\odot} \text{yr}^{-1}$. Already mild dust-attenuation in the host can easily increase this to values of $50 M_{\odot} \text{yr}^{-1}$ or even higher, illustrating that GRB hosts with SFRs significantly above $10 M_{\odot} \text{yr}^{-1}$ are not an exceptionally rare phenomenon at $z > 1$ (see also e.g., Fynbo et al. 2005; Chen et al. 2011; Krühler et al. 2011; Savaglio et al. 2012).

4.2. Afterglow versus host properties

The substantial gas-phase metallicity of $Z \sim Z_{\odot}/2$ might directly relate to the substantial $A_V \sim 0.5$ mag including the presence of the 2175 Å dust feature as observed in the afterglow SED (Greiner et al. 2011) and spectrum (Zafar et al. 2012). A metallicity of around solar was also inferred from GRB-DLAs for GRBs 070802 and 080607, both of which were substantially reddened, and had 2175 Å dust features (Elíasdóttir et al. 2009; Prochaska et al. 2009; Perley et al. 2011b) as well. This seems to support the association between the 2175 Å bump and chemically evolved galaxies (e.g., Noll et al. 2009). With only a small handful of such events, however, no strong conclusions can be drawn, yet.

4.3. The mass-metallicity relation at $z \sim 2$

Having the key parameters of stellar mass, metallicity and SFR of the host of GRB 080605 at hand, we can now investigate its relation to the mass-metallicity ($M_* - Z$) relation at $z \sim 2$ (e.g., Erb et al. 2006). A further basic property is the host’s location with respect to the fundamental metallicity relation (FMR) defined by SDSS galaxies in a mass range between $9.2 \leq \log(M_*) \leq 11.4$. The FMR connects M_* , $12 + \log(\text{O}/\text{H})$, and SFR (Mannucci et al. 2010) via:

$$12 + \log(\text{O}/\text{H}) = 8.90 + 0.47 \times (\mu_{0.32} - 10) \quad (2)$$

where $\mu_{0.32} = \log(M_* [M_{\odot}]) - 0.32 \times \log(\text{SFR}_{\text{H}\alpha} [M_{\odot} \text{yr}^{-1}])$. The oxygen abundance for GRB 080605 on the Mannucci et al. (2010, 2011) scale is $12 + \log(\text{O}/\text{H}) = 8.52 \pm 0.09$. The value derived from M_* and SFR via Eq. (2) is consistent with it ($12 + \log(\text{O}/\text{H}) = 8.63 \pm 0.08$). Errors are again based on the statistical uncertainty of line-flux measurement, correction factor and stellar mass only⁷.

This establishes the host of GRB 080605 as a star-forming galaxy which has no significant deficit of metals with respect to star-forming galaxies at low redshift for its given mass and SFR. Or, conversely, the selection through the energetic GRB 080605 does not lead to its host being metal-poor with respect to field galaxies of comparable stellar mass and SFR.

The host of GRB 080605 hence provides the opportunity to probe the mass-metallicity relation at $z \sim 2$ (e.g., Erb et al. 2006) at lower stellar masses (Fig. 6). If populated with more events, GRB hosts can thus provide unique constraints on the low-mass end of the $M_* - Z$ relation (see also e.g., Vergani et al. 2011)

⁷ A systematic error on the stellar mass estimate of ± 0.2 dex., for example, would translate into additional systematic errors of ± 0.12 on the derived metallicity.

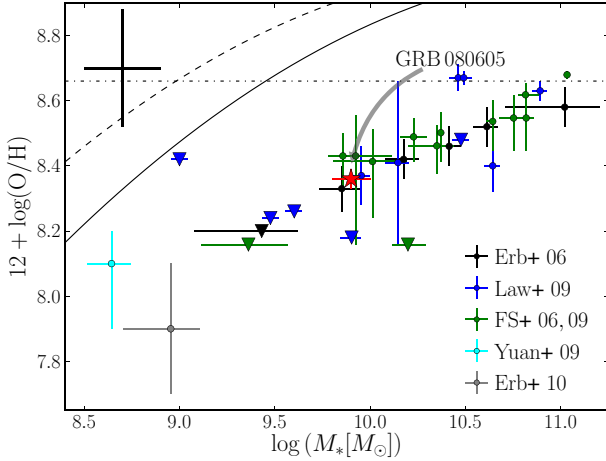


Fig. 6. The host of GRB 080605 with respect to the mass–metallicity relation at $z \sim 2$. Different colored symbols represent the averaged galaxy distribution from Erb et al. (2006) in black, as well as individual sources from Förster Schreiber et al. (2006, 2009) in green, from Law et al. (2009) in blue and gravitationally lensed galaxies from Yuan & Kewley (2009) and Erb et al. (2010) in cyan and gray, respectively. Upper limits are shown with downward triangles with the same color-coding. All measurements are in the N2 scale of Pettini & Pagel (2004). The horizontal dashed-dotted line marks the solar oxygen abundance. The dashed line is the local $M-Z$ relation (Tremonti et al. 2004), which is also shown shifted (solid line) to the observations at $z \sim 0.7$ (Savaglio et al. 2005). Approximate systematic errors on the N2 metallicity scale and the mass determination are indicated in the top left corner.

similar to measurements via gravitationally lensed objects (e.g., Wuyts et al. 2012) but without the need for (and uncertainty of) a detailed lens model (Fig. 6).

4.4. The non-detection of $\text{Ly}\alpha$

The luminosity-independent selection of star-forming galaxies through GRBs offers a unique probe of the escape fraction (f_{esc}) of $\text{Ly}\alpha$ photons. The path length of resonantly scattered $\text{Ly}\alpha$ photons depends on the geometry and kinematics of H I within a galaxy, and could thus be greatly enhanced as compared to, for example, the path length of photons from recombination lines such as $\text{H}\alpha$. The longer path length directly translates into a higher dust absorption probability for $\text{Ly}\alpha$ photons and hence f_{esc} might end up anywhere below unity (e.g., Atek et al. 2009).

$\text{Ly}\alpha$ emission from GRB hosts was detected in both narrow-band imaging and afterglow/host spectroscopy (e.g., Fynbo et al. 2003; Jakobsson et al. 2005; D’Avanzo et al. 2010; Milvang-Jensen et al. 2012). The broad wavelength coverage of X-shooter extending down to the UV ($\text{Ly}\alpha$ line at $z \sim 1.64$ is redshifted to 3210 Å) coupled with the tight constraints on the galaxies reddening and extreme luminosity of $\text{H}\alpha$, makes the host of GRB 080605 an ideal test case for the escape fraction in a high-redshift environment.

At $f_{\text{esc}} = 1$, the intrinsic ratio between $\text{Ly}\alpha$ and $\text{H}\alpha$ is 8.7 (Brocklehurst 1971). Consequently, $\text{Ly}\alpha$ is expected to be a factor 12 more luminous than our non-detection implies. This corresponds to an escape fraction of $f_{\text{esc}} < 0.08$, which was estimated in the same way as the flux limit but using the photometry-matched spectrum and its errors as discussed in Sect. 2.3.

While the evidence for reddening from the recombination lines and the stellar continuum is weak, the properties of the afterglow (Zafar et al. 2012) provide compelling evidence

that there is enough dust in the ISM to absorb the scattered $\text{Ly}\alpha$ photons efficiently.

Our limit is consistent with previous estimates using narrow-band surveys targeting both $\text{Ly}\alpha$ and $\text{H}\alpha$ (Hayes et al. 2010) or measured from the column density distribution of GRB-DLAs (Fynbo et al. 2009). A larger sample of hosts observed in similar fashion can provide competitive constraints on the average escape fraction in high-redshift environments at $1.6 < z < 2.5$. These measurements would be completely independent on conventional selection techniques, and representative of young, star-forming galaxies common in the early Universe. Establishing the average escape fraction at cosmological distances and for typical star-forming galaxies has strong implications for the use of $\text{Ly}\alpha$ emission as a tracer of star-formation and luminosity functions derived from $\text{Ly}\alpha$ galaxies at the highest redshifts.

5. Conclusions

We presented medium-resolution optical/NIR spectroscopy and ground- and space-based imaging of the galaxy selected through GRB 080605 at $z = 1.64$. Our HST imaging probes and resolves the large-scale structure of the host, and shows it to be a morphologically complex system that consists of two components separated by 8.6 kpc. An X-shooter spectrum covering its rest-frame UV-to optical wavelength range (1150 to 8700 Å) reveals a wealth of emission lines, including [O II], [O III], $\text{H}\beta$ as well as [N II] and $\text{H}\alpha$. These recombination and forbidden lines allow us to put unique constraints on the conditions of the ISM in the host. It is in particular the first robust measurement of the gas-phase metallicity of a GRB host at $z > 1$ using strong-line indicators based on [N II] ($\lambda 6584$).

The host of GRB 080605 is significantly enriched with metals with an oxygen abundance $12 + \log(\text{O}/\text{H})$ between 8.3 and 8.6 ($0.4 Z_{\odot} < Z < 0.8 Z_{\odot}$) for several different strong-line diagnostics. In addition, its stellar mass is $M_* = 8.0^{+1.3}_{-1.6} \times 10^9 M_{\odot}$ and the galaxy is extremely star-forming ($\text{SFR}_{\text{H}\alpha} = 31^{+12}_{-6} M_{\odot} \text{yr}^{-1}$, $\text{sSFR}_{\text{H}\alpha} = 4 \text{Gyr}^{-1}$). With a gas-phase metallicity above 40% of the solar value and luminosity above L^* (Krühler et al. 2011), it contrasts many observation of GRBs at lower redshift, which typically showed their hosts to be sub-luminous and metal-poor galaxies. Coupled with the high energy-release in γ -rays of $E_{\gamma, \text{iso}} \sim 2.2 \times 10^{53} \text{erg}$, it challenges those GRB progenitor models in which the formation of energetic GRBs requires very low metallicities.

The metallicity measurement of the host of GRB 080605 directly shows that GRB hosts at $z > 1$ are not necessarily metal-poor, both on absolute scales as well as relative to their stellar mass and SFR. Our detailed spectroscopic observations in fact suggest that the hosts of GRBs in general might provide a fair representation of the high-redshift, SFR-weighted population of ordinary star-forming galaxies.

GRB hosts thus offer a selection of star-forming galaxies at high redshifts, including objects in the low-mass ($M_* \lesssim 10^{10} M_{\odot}$) regime, which are challenging to study otherwise. Targeted spectroscopic investigation become feasible through the afterglow’s redshift, its sub-arcsec position and the substantial star-formation within GRB-selected galaxies.

Similar data for a representative and statistically significant sample of GRB hosts hold the key for understanding the nature of GRB hosts in particular and give important insights into the high-redshift population of star-forming galaxies in general. Furthermore, they yield the fundamental information to establish GRBs as probes of the star-formation up to the

era of re-ionization. With the availability of highly redshift-complete GRB, afterglow and host samples such as TOUGH⁸ (Hjorth et al. 2012; Jakobsson et al. 2012; Milvang-Jensen et al. 2012; Krühler et al. 2012; Michałowski et al. 2012, Malesani et al., in prep.) and NIR spectroscopy with X-shooter these studies are now feasible for the first time, and will continue to open the window with respect to the properties of GRB hosts in the previously unexplored redshift range $1 \lesssim z \lesssim 3$.

Acknowledgements. We thank L. Christensen and S. Savaglio for important insights and valuable discussion, and A. Rau for providing data for Fig. 5 in machine-readable format. We also thank the referee for constructive comments, that helped to improve the quality of the manuscript. T.K. acknowledges support by the European Commission under the Marie Curie Intra-European Fellowship Programme in FP7. J.P.U.F. acknowledges support from the ERC-StG grant EGG5-278202. The Dark Cosmology Centre is funded by the Danish National Research Foundation. Based on observations made with the NASA/ESA *Hubble* Space Telescope, obtained from the data archive at the Space Telescope Institute.

References

- Alloin, D., Collin-Souffrin, S., Joly, M., & Vigroux, L. 1979, *A&A*, 78, 200
- Arnouts, S., Cristiani, S., Moscardini, L., et al. 1999, *MNRAS*, 310, 540
- Asplund, M., Grevesse, N., Sauval, A. J., & Scott, P. 2009, *ARA&A*, 47, 481
- Atek, H., Kunth, D., Schaerer, D., et al. 2009, *A&A*, 506, L1
- Basa, S., Cuby, J. G., Savaglio, S., et al. 2012, *A&A*, 542, 103
- Berger, E., Cowie, L. L., Kulkarni, S. R., et al. 2003, *ApJ*, 588, 99
- Berger, E., Fox, D. B., Kulkarni, S. R., Frail, D. A., & Djorgovski, S. G. 2007, *ApJ*, 660, 504
- Bertin, E., & Arnouts, S. 1996, *A&AS*, 117, 393
- Brocklehurst, M. 1971, *MNRAS*, 153, 471
- Bruzual, G., & Charlot, S. 2003, *MNRAS*, 344, 1000
- Calzetti, D. 2001, *PASP*, 113, 1449
- Butler, N. R., Kocevski, D., Bloom, J. S., & Curtis, J. L. 2007, *ApJ*, 671, 656
- Butler, N. R., Bloom, J. S., & Poznanski, D. 2010, *ApJ*, 711, 495
- Campana, S., Mangano, V., Blustin, A. J., et al. 2006, *Nature*, 442, 1008
- Campisi, M. A., Tapparello, C., Salvaterra, R., Mannucci, F., & Colpi, M. 2011, *MNRAS*, 417, 1013
- Cardelli, J. A., Clayton, G. C., & Mathis, J. S. 1989, *ApJ*, 345, 245
- enko, S. B., Kelemen, J., Harrison, F. A., et al. 2009, *ApJ*, 693, 1484
- Chabrier, G. 2003, *PASP*, 115, 763
- Chen, H.-W. 2012, *MNRAS*, 419, 3039
- Chen, H., Perley, D. A., Pollack, L. K., et al. 2009, *ApJ*, 691, 152
- Chen, H., Perley, D. A., Wilson, C. D., et al. 2011, *ApJ*, 727, L53
- Christensen, L., Hjorth, J., & Gorosabel, J. 2004, *A&A*, 425, 913
- Christensen, L., Vreeswijk, P. M., Sollerman, J., et al. 2008, *A&A*, 490, 45
- Christensen, L., D'Odorico, S., Pettini, M., et al. 2010, *MNRAS*, 406, 2616
- Clemens, C., Krühler, T., Greiner, J., et al. 2008, *GCN*, 7834
- Copetti, M. V. F., Mallmann, J. A. H., Schmidt, A. A., & Castañeda, H. O. 2000, *A&A*, 357, 621
- Cowie, L. L., & Barger, A. J. 2008, *ApJ*, 686, 72
- Cucchiara, A., Levan, A. J., Fox, D. B., et al. 2011, *ApJ*, 736, 7
- D'Avanzo, P., Perri, M., Fugazza, D., et al. 2010, *A&A*, 522, A20
- de Ugarte Postigo, A., Goldoni, P., Thöne, C. C., et al. 2010, *A&A*, 513, A42
- D'Elia, V., Fynbo, J. P. U., Covino, S., et al. 2010, *A&A*, 523, A36
- Dessauges-Zavadsky, M., D'Odorico, S., Schaerer, D., et al. 2010, *A&A*, 510, A26
- D'Odorico, S., Dekker, H., Mazzoleni, R., et al. 2006, in *SPIE Conf. Ser.*, 6269
- Draine, B. T. 2003, *ARA&A*, 41, 241
- Elíasdóttir, Á., Fynbo, J. P. U., Hjorth, J., et al. 2009, *ApJ*, 697, 1725
- Elliott, J., Greiner, J., Khochfar, S., et al. 2012, *A&A*, 539, 113
- Erb, D. K., Shapley, A. E., Pettini, M., et al. 2006, *ApJ*, 644, 813
- Erb, D. K., Pettini, M., Shapley, A. E., et al. 2010, *ApJ*, 719, 1168
- Förster Schreiber, N. M., Genzel, R., Lehnert, M. D., et al. 2006, *ApJ*, 645, 1062
- Förster Schreiber, N. M., Genzel, R., Bouché, N., et al. 2009, *ApJ*, 706, 1364
- Fruchter, A. S., Levan, A. J., Strolger, L., et al. 2006, *Nature*, 441, 463
- Fryer, C. L., Woosley, S. E., & Hartmann, D. H. 1999, *ApJ*, 526, 152
- Fynbo, J. P. U., Jensen, B. L., Gorosabel, J., et al. 2001, *A&A*, 369, 373
- Fynbo, J. P. U., Jakobsson, P., Möller, P., et al. 2003, *A&A*, 406, L63
- Fynbo, J. P. U., Gorosabel, J., Smette, A., et al. 2005, *ApJ*, 633, 317
- Fynbo, J. P. U., Jakobsson, P., Prochaska, J. X., et al. 2009, *ApJS*, 185, 526
- Fynbo, J. P. U., Laursen, P., Ledoux, C., et al. 2010, *MNRAS*, 408, 2128
- Galama, T. J., & Wijers, R. A. M. J. 2001, *ApJ*, 549, L209
- Galama, T. J., Vreeswijk, P. M., van Paradijs, J., et al. 1998, *Nature*, 395, 670
- Gehrels, N., Chincarini, G., Giommi, P., et al. 2004, *ApJ*, 611, 1005
- Gehrels, N., Ramirez-Ruiz, E., & Fox, D. B. 2009, *ARA&A*, 47, 567
- Goldoni, P., Royer, F., François, P., et al. 2006, in *SPIE Conf. Ser.*, 6269
- Golenetskii, S., Aptekar, R., Mazets, E., et al. 2008, *GCN*, 7854
- Graham, A. W., & Driver, S. P. 2005, *PASA*, 22, 118
- Graham, J. F., Fruchter, A. S., Kewley, L. J., et al. 2009, in *AIPC Ser.*, 1133, 269
- Greiner, J., Bornemann, W., Clemens, C., et al. 2008, *PASP*, 120, 405
- Greiner, J., Krühler, T., Fynbo, J. P. U., et al. 2009, *ApJ*, 693, 1610
- Greiner, J., Krühler, T., Klose, S., et al. 2011, *A&A*, 526, A30
- Groot, P. J., Galama, T. J., van Paradijs, J., et al. 1998, *ApJ*, 493, L27
- Hayashi, M., Motohara, K., Shimasaku, K., et al. 2009, *ApJ*, 691, 140
- Hayes, M., Östlin, G., Schaerer, D., et al. 2010, *Nature*, 464, 562
- Hirschi, R., Meynet, G., & Maeder, A. 2005, *A&A*, 443, 581
- Hjorth, J., Sollerman, J., Möller, P., et al. 2003, *Nature*, 423, 847
- Hjorth, J., Malesani, D., Jakobsson, P., et al. 2012, *ApJ*, 756, 187
- Hunt, L., Palazzi, E., Rossi, A., et al. 2011, *ApJ*, 736, L36
- Ilbert, O., Arnouts, S., McCracken, H. J., et al. 2006, *A&A*, 457, 841
- Jakobsson, P., Björnsson, G., Fynbo, J. P. U., et al. 2005, *MNRAS*, 362, 245
- Jakobsson, P., Fynbo, J. P. U., Ledoux, C., et al. 2006, *A&A*, 460, L13
- Jakobsson, P., Vreeswijk, P. M., Xu, D., & Thöne, C. C. 2008, *GCN*, 7832
- Jakobsson, P., Hjorth, J., Malesani, D., 2012, et al. 2012, *ApJ*, 752, 62
- Kann, D. A., Klose, S., & Zeh, A. 2006, *ApJ*, 641, 993
- Kann, D. A., Laux, U., Klose, S., Ertel, S., & Greiner, J. 2008, *GCN*, 7829
- Kauffmann, G., Heckman, T. M., Tremonti, C., et al. 2003, *MNRAS*, 346, 1055
- Kennicutt, Jr., R. C. 1998, *ARA&A*, 36, 189
- Kewley, L. J., & Dopita, M. A. 2002, *ApJS*, 142, 35
- Kewley, L. J., & Ellison, S. L. 2008, *ApJ*, 681, 1183
- Kewley, L. J., Dopita, M. A., Sutherland, R. S., Heisler, C. A., & Trevena, J. 2001, *ApJ*, 556, 121
- Kewley, L. J., Geller, M. J., & Jansen, R. A. 2004, *AJ*, 127, 2002
- Kistler, M. D., Yüksel, H., Beacom, J. F., Hopkins, A. M., & Wyithe, J. S. B. 2009, *ApJ*, 705, L104
- Kobulnicky, H. A., & Kewley, L. J. 2004, *ApJ*, 617, 240
- Kocevski, D., & West, A. A. 2011, *ApJ*, 735, L8
- Kocevski, D., West, A. A., & Modjaz, M. 2009, *ApJ*, 702, 377
- Krühler, T., Küpcü Yoldaş, A., Greiner, J., et al. 2008, *ApJ*, 685, 376
- Krühler, T., Greiner, J., Schady, P., et al. 2011, *A&A*, 534, A108
- Krühler, T., Malesani, D., Milvang-Jensen, B., et al. 2012, *ApJ*, in press [arXiv:1205.4036]
- Lara-López, M. A., Cepa, J., Bongiovanni, A., et al. 2010, *A&A*, 521, L53
- Law, D. R., Steidel, C. C., Erb, D. K., et al. 2009, *ApJ*, 697, 2057
- Levan, A., Fruchter, A., Rhoads, J., et al. 2006, *ApJ*, 647, 471
- Levesque, E. M., Berger, E., Kewley, L. J., & Bagley, M. M. 2010a, *AJ*, 139, 694
- Levesque, E. M., Soderberg, A. M., Kewley, L. J., & Berger, E. 2010b, *ApJ*, 725, 1337
- Levesque, E. M., Berger, E., Soderberg, A. M., & Chornock, R. 2011, *ApJ*, 739, 23
- MacFadyen, A. I., & Woosley, S. E. 1999, *ApJ*, 524, 262
- Maiolino, R., Nagao, T., Grazian, A., et al. 2008, *A&A*, 488, 463
- Malesani, D., Tagliaferri, G., Chincarini, G., et al. 2004, *ApJ*, 609, L5
- Malesani, D., Hjorth, J., Fynbo, J. P. U., et al. 2009, in *AIPC Ser.*, 1111, 513
- Manchado, A., Barreto, M., Acosta-Pulido, J., et al. 2004, in *SPIE Conf. Ser.*, 5492, 1094
- Mannucci, F., Cresci, G., Maiolino, R., et al. 2009, *MNRAS*, 398, 1915
- Mannucci, F., Cresci, G., Maiolino, R., Marconi, A., & Gnerucci, A. 2010, *MNRAS*, 408, 2115
- Mannucci, F., Salvaterra, R., & Campisi, M. A. 2011, *MNRAS*, 414, 1263
- McCall, M. L., Rybski, P. M., & Shields, G. A. 1985, *ApJS*, 57, 1
- McGaugh, S. S. 1991, *ApJ*, 380, 140
- Michałowski, M. J., Hjorth, J., Castro Cerón, J. M., & Watson, D. 2008, *ApJ*, 672, 817
- Michałowski, M., Kamble, A., Hjorth, J., et al. 2012, *ApJ*, 755, 85
- Milvang-Jensen, B., Fynbo, J. P. U., Malesani, D., et al. 2012, *ApJ*, 756, 25
- Modjaz, M., Kewley, L., Kirshner, R. P., et al. 2008, *AJ*, 135, 1136
- Nagao, T., Maiolino, R., & Marconi, A. 2006, *A&A*, 459, 85
- Noll, S., Pierini, D., Cimatti, A., et al. 2009, *A&A*, 499, 69
- Osterbrock, D. E. 1989, *Astrophysics of gaseous nebulae and active galactic nuclei* (University Science Books)
- Osterbrock, D. E., & Ferland, G. J. 2006, *Astrophysics of gaseous nebulae and active galactic nuclei* (University Science Books)
- Pagel, B. E. J., Edmunds, M. G., Blackwell, D. E., Chun, M. S., & Smith, G. 1979, *MNRAS*, 189, 95
- Pei, Y. C. 1992, *ApJ*, 395, 130
- Pérez-Montero, E., Contini, T., Lamareille, F., et al. 2009, *A&A*, 495, 73
- Perley, D. A., Cenko, S. B., Bloom, J. S., et al. 2009, *AJ*, 138, 1690

⁸ <http://www.dark-cosmology.dk/TOUGH>

- Perley, D. A., Bloom, J. S., Cenko, S. B., et al. 2011a, in AAS Meeting Abstracts, 217, 108.02
- Perley, D. A., Morgan, A. N., Updike, A., et al. 2011b, *AJ*, 141, 36
- Pettini, M., & Pagel, B. E. J. 2004, *MNRAS*, 348, L59
- Pian, E., Mazzali, P. A., Masetti, N., et al. 2006, *Nature*, 442, 1011
- Pierini, D., Gordon, K. D., Witt, A. N., & Madsen, G. J. 2004, *ApJ*, 617, 1022
- Piran, T. 2004, *Rev. Mod. Phys.*, 76, 1143
- Pontzen, A., Deason, A., Governato, F., et al. 2010, *MNRAS*, 402, 1523
- Prochaska, J. X., Gawiser, E., Wolfe, A. M., Cooke, J., & Gelino, D. 2003, *ApJS*, 147, 227
- Prochaska, J. X., Chen, H., & Bloom, J. S. 2006, *ApJ*, 648, 95
- Prochaska, J. X., Dessauges-Zavadsky, M., Ramirez-Ruiz, E., & Chen, H.-W. 2008, *ApJ*, 685, 344
- Prochaska, J. X., Sheffer, Y., Perley, D. A., et al. 2009, *ApJ*, 691, L27
- Rau, A., Savaglio, S., Krühler, T., et al. 2010, *ApJ*, 720, 862
- Richard, J., Jones, T., Ellis, R., et al. 2011, *MNRAS*, 413, 643
- Robertson, B. E., & Ellis, R. S. 2012, *ApJ*, 744, 95
- Rossi, A., Klose, S., Ferrero, P., et al. 2012, *A&A*, 545, A77
- Salvaterra, R., Della Valle, M., Campana, S., et al. 2009, *Nature*, 461, 1258
- Salvaterra, R., Campana, S., Vergani, S. D., et al. 2012, *ApJ*, 749, 68
- Savaglio, S. 2006, *New J. Phys.*, 8, 195
- Savaglio, S., Fall, S. M., & Fiore, F. 2003, *ApJ*, 585, 638
- Savaglio, S., Glazebrook, K., Le Borgne, D., et al. 2005, *ApJ*, 635, 260
- Savaglio, S., Glazebrook, K., & Le Borgne, D. 2009, *ApJ*, 691, 182
- Savaglio, S., Rau, A., Greiner, J., et al. 2012, *MNRAS*, 420, 627
- Sbarufatti, B., Barthelmy, S. D., Burrows, D. N., et al. 2008, *GCN*, 7828
- Schady, P., Mason, K. O., Page, M. J., et al. 2007, *MNRAS*, 377, 273
- Schady, P., Page, M. J., Oates, S. R., et al. 2010, *MNRAS*, 401, 2773
- Schady, P., Dwelly, T., Page, M. J., et al. 2012, *A&A*, 537, A15
- Schlegel, D. J., Finkbeiner, D. P., & Davis, M. 1998, *ApJ*, 500, 525
- Stanek, K. Z., Matheson, T., Garnavich, P. M., et al. 2003, *ApJ*, 591, L17
- Stanek, K. Z., Gnedin, O. Y., Beacom, J. F., et al. 2006, *Acta Astron.*, 56, 333
- Svensson, K. M., Tanvir, N. R., Perley, D. A., et al. 2012, *MNRAS*, 421, 25
- Tanvir, N. R., Barnard, V. E., Blain, A. W., et al. 2004, *MNRAS*, 352, 1073
- Tanvir, N. R., Fox, D. B., Levan, A. J., et al. 2009, *Nature*, 461, 1254
- Tanvir, N. R., Levan, A. J., Fruchter, A. S., et al. 2012, *ApJ*, 754, 46
- Thöne, C. C., Fynbo, J. P. U., Östlin, G., et al. 2008, *ApJ*, 676, 1151
- Thöne, C. C., Fynbo, J. P. U., Goldoni, P., et al. 2012, unpublished [arXiv:1206.2337]
- Tody, D. 1993, in *Astronomical Data Analysis Software and Systems II*, ASPC Ser., 52, 173
- Tremonti, C. A., Heckman, T. M., Kauffmann, G., et al. 2004, *ApJ*, 613, 898
- Vergani, S. D., Flores, H., Covino, S., et al. 2011, *A&A*, 535, A127
- Vernet, J., Dekker, H., D'Odorico, S., et al. 2011, *A&A*, 536, A105
- Vreeswijk, P. M., Ellison, S. L., Ledoux, C., et al. 2004, *A&A*, 419, 927
- Watson, D., French, J., Christensen, L., et al. 2011, *ApJ*, 741, 58
- Wolf, C., & Podsiadlowski, P. 2007, *MNRAS*, 375, 1049
- Woosley, S. E. 1993, *ApJ*, 405, 273
- Wuyts, E., Rigby, J. R., Sharon, K., & Gladders, M. D. 2012, *ApJ*, 755, 73
- Yoon, S., & Langer, N. 2005, *A&A*, 443, 643
- Yuan, T.-T., & Kewley, L. J. 2009, *ApJ*, 699, L161
- Zafar, T., Watson, D., Fynbo, J. P. U., et al. 2011, *A&A*, 532, A143
- Zafar, T., Watson, D., Elíasdóttir, Á., Fynbo, J. P. U., et al. 2012, *ApJ*, 753, 82
- Zahid, H. J., Kewley, L. J., & Bresolin, F. 2011, *ApJ*, 730, 137